STEM CELLS®

TISSUE-SPECIFIC STEM CELLS

mDia1 and Cdc42 Regulate Activin B-Induced Migration of Bone Marrow-Derived Mesenchymal Stromal Cells

XUEER WANG,[a] PEI TANG,[a] FUKUN GUO,[c] MIN ZHANG,[a] YUAN YAN,[a] MIANBO HUANG,[a] YINGHUA CHEN,[a] LU ZHANG,[b] LIN ZHANG[a]

[a]Guangdong Provincial Key Laboratory of Tissue Construction and Detection, School of Basic Medical Sciences, Southern Medical University, Guangzhou, People's Republic of China; [b]Guangdong Provincial Key Laboratory of Proteomics, Key Laboratory of Mental Health of the Ministry of Education, School of Basic Medical Sciences, Southern Medical University, Guangzhou, People's Republic of China; [c]Division of Experimental Hematology and Cancer Biology, Children's Hospital Research Foundation, Cincinnati, Ohio, USA

Correspondence: Lin Zhang, Ph.D., Guangdong Provincial Key Laboratory of Tissue Construction and Detection, School of Basic Medical Sciences, Southern Medical University, 1838 Guangzhou Avenue North, Guangzhou 510515, People's Republic of China. Telephone: 8602061648205; e-mail: zlilyzh@126.com; or Lu Zhang, Ph.D., Guangdong Provincial Key Laboratory of Proteomics, Key Laboratory of Mental Health of the Ministry of Education, School of Basic Medical Sciences, Southern Medical University, 1838 Guangzhou Avenue North, Guangzhou 510515, People's Republic of China. Telephone: 8602061648726; e-mail: zlulu70@126.com

Received June 16, 2018; accepted for publication August 28, 2018; first published online in STEM CELLS *EXPRESS* October 24, 2018.

http://dx.doi.org/10.1002/stem.2924

Key Words. Bone marrow stromal cells • Cell migration • Cell signaling • Cell transplantation • Mesenchymal stem cells

ABSTRACT

In a previous study, we have shown that Activin B is a potent chemoattractant for bone marrow-derived mesenchymal stromal cells (BMSCs). As such, the combination of Activin B and BMSCs significantly accelerated rat skin wound healing. In another study, we showed that RhoA activation plays a key role in Activin B-induced BMSC migration. However, the role of the immediate downstream effectors of RhoA in this process is unclear. Here, we demonstrated that mammalian homolog of Drosophila diaphanous-1 (mDia1), a downstream effector of RhoA, exerts a crucial function in Activin B-induced BMSC migration by promoting membrane ruffling, microtubule morphology, and adhesion signaling dynamics. Furthermore, we showed that Activin B does not change Rac1 activity but increases Cdc42 activity in BMSCs. Inactivation of Cdc42 inhibited Activin B-stimulated Golgi reorientation and the cell migration of BMSCs. Furthermore, knockdown of mDia1 affected Activin B-induced BMSC-mediated wound healing in vivo. In conclusion, this study demonstrated that the RhoA-mDia1 and Cdc42 pathways regulate Activin B-induced BMSC migration. This study may help to optimize clinical MSC-based transplantation strategies to promote skin wound healing. STEM CELLS *2019;37:150–161*

SIGNIFICANCE STATEMENT

This study demonstrates that the RhoA-mDia1 pathway exerts a crucial function in Activin B-induced bone marrow-derived mesenchymal stromal cell (BMSC) migration by regulating membrane ruffle formation, microtubule morphology, and focal adhesion signaling dynamics. Cdc42 regulates Activin B-induced Golgi reorientation at the leading edge of moving BMSCs. Knockdown of mDia1 affects Activin B-induced BMSC-mediated wound healing in vivo. This study has revealed new molecular mechanisms of BMSC migration that will help optimize MSC-based transplantation strategies in clinical skin wound healing.

INTRODUCTION

Bone marrow-derived mesenchymal stromal cells (BMSCs) have been reported to possess the capacity to differentiate into multiple cell types [1]. BMSC administration was shown to have a beneficial effect on cutaneous wound repair by accelerating wound healing, increasing epithelialization, and promoting granulation formation [2–4].

In a previous study, we showed that Activin B, a member of the transforming growth factor β (TGFβ) superfamily [5], exerted a beneficial effect on BMSC-mediated wound repair: in vivo, the combination of Activin B and BMSCs promoted rat skin wound healing, and in vitro, Activin B promoted the migration and stress fiber formation of BMSCs [6]. Because migration of BMSCs toward wound sites is crucial for clinical applications, elucidation of BMSC migration will help modulate expansion protocols to obtain cells that maintain their migratory capacities.

RhoA, a member of the Rho family GTPases, plays an important role in cell migration by controlling protrusion, adhesion, and contraction [7, 8]. RhoA functions by binding to and activating its immediate downstream effectors [9]. Rho-associated protein kinase (ROCK) and mammalian homolog of Drosophila diaphanous-1 (mDia1) are two major effector proteins of RhoA [10]. In a further study, we demonstrated that although RhoA was important for both Activin B-induced stress fiber formation and the cell movement of BMSCs, ROCK promoted stress fiber formation but suppressed BMSC migration [11]. These findings suggest that stress fiber formation is not likely to count for Activin

B-induced BMSC migration and that RhoA regulates Activin B-induced stress fiber formation dependent on ROCK but cell migration independent of ROCK in BMSCs [11]. Therefore, in this study, we explored other downstream effectors of RhoA and other mechanisms for their potential role in BMSC migration induced by Activin B.

In this study, by using a small interfering RNA (siRNA) of mDia1, we detected the function of mDia1 in Activin B-induced membrane ruffling, microtubule morphology, focal adhesion signaling dynamics, and migration of BMSCs. Moreover, we investigated the role of other members of the Rho GTPases, Rac1, and Cdc42, in Activin B-induced BMSC migration. Finally, we detected the effect of mDia1 in Activin B-induced BMSC-mediated skin wound healing in vivo.

Materials and Methods

All animal procedures were approved by the Institutional Animal Care and Use Committee at Southern Medical University (No. 2015-063).

Isolation, Culture, and Identification of BMSCs

BMSC isolation was performed as previously described [6, 11, 12]. In brief, MSCs were isolated from the bone marrow of 6-week-old male Sprague-Dawley rats, which were purchased from the Laboratory Animal Centre of Southern Medical University. Bone marrow was collected and centrifuged at 1,000 rpm for 5 minutes. The cell pellet was resuspended in complete medium (Dulbecco's modified Eagle's medium [DMEM] with 10% fetal bovine serum [FBS] and 1% antibiotic antimycotic solution) and cultured in 100-mm dishes at 37°C and 5% CO_2. Isolated BMSCs were characterized by immunocytochemistry as we previously described [6, 11]. Cells at passages 3–4 were used for all experiments.

siRNA Knockdown of mDia1

Two independent short interfering double-stranded RNA oligomers (siRNAs) of mDia1 (mDia1-siRNA [1; 5′-GCGACGGCGGCAAACATAAGAAATT-3′] and mDia1-siRNA [2; 5′-GCAGAAACTTCAGGATCTT-3′]) and negative control (NC) siRNA were designed and synthesized by RiboBio (Guangzhou, China). For siRNA transfection, 100 nM of each siRNA and Lipofectamine 3,000 (Invitrogen, Carlsbad, CA) were used according to the manufacturer's protocols. BMSCs were transfected with mDia1-siRNA (1), mDia1-siRNA (2), or NC for 24 hours or 48 hours in the experiments. The transfection efficiency of the siRNA was further confirmed by Western blotting.

Lentivirus Production and Infection

The lentiviral vector containing shRNA targeting Diaph1 was constructed by Obio Biotechnology (Shanghai, China). For construction of the shRNA vector, sense, and antisense oligonucleotides containing a 25-base sequence (5′-GCGACGGCGGCAAACATAAGAAATT-3′) targeting Diaph1 (GenBank accession number: NM_001107393) were annealed and ligated to the 3′ end of enhanced green fluorescent protein (EGFP) from the pLKD-CMV-EGFP-2A-Puro-U6-shRNA vector with interchanging recombination. All constructs were confirmed by sequencing. Lentivirus was produced by transfection of 293T cells with three plasmids: a lentiviral vector expressing Diaph1, shRNA targeting Diaph1 or EGFP alone, package helper plasmids pspax2 and pMD2G. Seventy-two hours after transfection, the supernatant was collected and purified by an ultracentrifugation method. The lentiviral titers were 7×10^7 TU/ml.

The dominant negative mutant Cdc42(N17), the constitutively active mutant Cdc42(L61), and the EGFP lentiviral vector were generated as described in our previous study [13]. The titers of Cdc42(N17), Cdc42(L61), and EGFP vector were 3.36×10^6 TU/ml, 2.19×10^6 TU/ml, and 2.24×10^6 TU/ml, respectively.

Cell Migration Assay

Cell migration was detected using the transwell assay and scratching wound healing assay as we previously reported [6, 11]. For the transwell assay, in brief, 100 μl of 50,000 treated or untreated BMSCs were plated in the upper compartment. Then, 600 μl of serum-free control medium with Activin B (10 ng/ml; R&D Systems, Minneapolis, MI) or not was added to the bottom chamber. After 24 hours, crystal violet was used to stain the cells that migrated to the lower chamber. Six visual fields (×20) were randomly selected to calculate the number of migrated cells in each group.

A scratch wound healing assay was adapted based on previously described methods [11, 14]. After the cells were transfected or treated, they were serum starved overnight. Then, the cells were detached and seeded in 12-well plates at a density of 1×10^5 cells/well. After scratching, the cells were cultured in the maintain-medium (DMEM with 1% FBS) with or without Activin B. Images were taken immediately and at 24 hours after scratching. Image-Pro Plus 6.0 software was used to calculate the scratching area.

Cell Proliferation Analysis

The Cell Counting Kit-8 (CCK8; Dojindo, Japan) assay was adopted to determine cell proliferation as previously described [11]. In brief, cells were plated in 96-well plates at a density of 1×10^4 cells/well. At the indicated times, 10 μl CCK8 solution was added to the well and incubated at 37°C for 2 hours. Each solution was measured spectrophotometrically at 450 nm.

Phalloidin Staining

Phalloidin staining protocols were adapted from previously described methods [6, 11]. To analyze the role of mDia1-siRNA on actin cytoskeleton reorganization in BMSC migration, the cells were firstly transfected with mDia1-siRNA (1) or NC for 24 hours. Then, the cells were serum starved overnight, followed by a scratching wound assay. After 8 hours of cell migration in the medium with or without Activin B, the cells were fixed and stained with Alexa Fluor 488 Phalloidin (1:40, Thermo Fisher, Invitrogen™, Carlsbad, CA, USA, A12379) for 45 minutes at room temperature and counterstained with 4′,6-Diamidino-2-Phenylindole (DAPI) (1:500; Sigma–Aldrich, St. Louis, MO) for 15 minutes. Then, images were acquired using a Leica DMi8 microscope.

To detect the effect of Cdc42 in actin reorganization, BMSCs were transfected with the EGFP vector, Cdc42(N17) or Cdc42(L61) for 48 hours. Then, the cells were seeded on a coverslip in each well of a 24-well plate at a density of 4×10^4 cells/well. The cells were serum starved overnight and then cultured in the maintain-medium in the presence or absence of Activin B for 4 hours. The cells were fixed and

stained with Alexa Fluor 546 Phalloidin (1:40, Thermo Fisher, A22283) and DAPI as previously described.

Microtubule Immunofluorescence Staining

The control group, mDia1-siRNA (1) group, Activin B group and mDia1-siRNA plus Activin B group were treated as described in the phalloidin staining procedures. BMSCs were cultured on coverslips in 24-well culture plates. At 8 hours after scratching, the cells were fixed and stained with primary α-tubulin antibody (1:200, Millipore, MAB1864-I, Billerica, MA) in 1% bovine serum albumin (BSA) overnight at 4°C, followed by incubation with donkey anti-rat secondary antibody (1:2,000; Thermo Fisher, Invitrogen, cat. #A-21208) in phosphate buffered saline with 0.05% Tween-20 (PBST) for 1 hour. After being washed, the cells were stained with DAPI. Images were acquired using a Leica DMi8 microscope.

Golgi Reorientation Analysis

BMSCs were transfected with siRNA or infected with lentivirus as described in the phalloidin staining procedures. The cells were starved overnight followed by in vitro scratching and treated with phosphate buffered solution (PBS) or Activin B. After 8 hours of cell migration, BMSCs were fixed. Primary GM130 (1:500, BD Transduction Laboratories, 610822, Lexington, KY) antibody was added and incubated overnight at 4°C. Then, the cells were incubated with goat anti-mouse secondary antibody (1:2,000; Invitrogen, cat. #35511) in PBS for 1 hour and counterstained with DAPI. Wood Ham's method was adopted to analyze the Golgi reorientation of cells [15]. Lines at a 120° angle representing the front 1/3 and rear 2/3 of the cell area were placed over the nuclei of all cells in the field of view. The number of cells with Golgi reorientation in the wound edge was counted manually. Cells were defined as positive if the Golgi was localized within a 120° sector facing directly toward the wound edge. More than 100 cells were evaluated for each experiment.

GST Pull Down Assay and Western Blot Analysis

To detect Rac1 and Cdc42 activation in BMSCs, a glutathione S-transferase (GST) pull-down assay (Rac/cdc42 Assay Reagent; Millipore, cat. #14-325) was performed according to the manufacturer's protocol as described previously [11, 13]. In brief, cell lysates were collected and GTP-bound Rac1 and Cdc42 were captured using immobilized PAK1-PBD agarose.

Western blotting was performed to analyze the activation and total levels of Cdc42 and Rac1 using the anti-Rac1 (1:500; BD Transduction Laboratories, 610651) and anti-Cdc42 antibody (1 μg/ml; Abcam, ab64533, Cambridge, U.K.), respectively, followed by the secondary antibody (1:1,000, Millipore, cat. #AP124P). For detection of endogenous mDia1 levels, the cell lysates were blotted with an anti-mDia1 antibody (1:1,000, BD Transduction Laboratories, 610848). For analysis of the focal adhesion complex, the cell lysates were blotted with anti-phospho (Tyr118; 1:1,000, Cell Signaling Technology, #2541, Beverly, MA) and total (1:4,000, BD Transduction Laboratories, 610051) paxillin and anti-phospho (Tyr397; 1:1,000, Invitrogen, 44-624G) and total (1:1,000, Invitrogen, 39-6500) focal adhesion kinase (FAK). The bands were visualized using the enhanced chemiluminescence (ECL) detection system. Quantity One software (Bio-Rad, Hercules, CA) was used to detect the band intensity.

Wound Healing Model

The wound healing model was established as we described previously [6]. Six-week-old Sprague-Dawley rats were divided into six treatment groups (n = 6 for each group). All groups had one square (1 cm × 1 cm) full-thickness wounds on both sides of the dorsal flank symmetrically. After wounding, the site surrounding the wound was treated with 0.5 ml PBS (PBS group), 10 ng/ml Activin B (ACT group), 6×10^6 per milliliter BMSCs (BMSC group), 10 ng/ml Activin B plus 6×10^6 per milliliter BMSCs (ACT + BMSC group), 6×10^6 per milliliter BMSCs transfected with lentivirus containing shRNA targeting mDia1 (BMSC[mDia1-shRNA] group), or 10 ng/ml Activin B plus 6×10^6 per milliliter BMSCs transfected with lentivirus containing shRNA targeting mDia1 (ACT + BMSC[mDia1-shRNA] group). The cells and/or growth factors were resuspended in 0.5 ml PBS and administered to the wounds by intradermal injection. The needle was inserted at the edge of the wound, and the cells or growth factors were injected into the center of the wound. After treatment, each rat was individually housed and fed ad libitum. Images were obtained at 0, 3, 7, and 14 days after wounding. Image-Pro Plus software was used to calculate the wound area. The wound closure rate was calculated as we previously described [6].

Hematoxylin and Eosin Staining and Histological Evaluation

The wounds and surrounding tissues were collected from the rats at 14 days post-treatment. The specimens were rinsed in PBS, fixed in 4% paraformaldehyde (PFA), dehydrated in a graded ethanol series, and embedded in paraffin. For the histological assessment, serial sections (5-μm) were collected and stained with hematoxylin and eosin staining according to standard procedures. Each slide was evaluated and given a histological score ranging from 1 to 3 according to re-epithelialization and granulation tissue formation. The criteria used for histological scores of wound healing were referred to previous researches [16–18] and summarized in Supporting Information Table S1. Six samples were selected from each group for evaluation.

Frozen Sections

For analysis of the applied BMSCs within the rat tissue, BMSCs were transfected with lentivirus containing EGFP vector or shRNA targeting mDia1 for 72 hours. On day 3 after cell transplantation, the wound and surrounding tissue was collected and divided in half. Tissues were frozen with optimal cutting temperature (OCT) compound. Serial sections (15 μm) were taken from the wound center to the edge by a freezing microtome at a controlled temperature of −20°C and adhered to the slides. Tissue sections were washed with PBS and blocked in PBS containing 2% BSA. The sections were stained with primary rabbit polyclonal anti-GFP antibody (1:200; Abcam) at 4°C overnight and secondary donkey anti-rabbit Alexa 488 antibody (1:200; Invitrogen) in PBS for 1 hour at room temperature. After counterstaining with DAPI for 10 minutes, the slides were examined by fluorescence microscopy.

Statistical Analyses

The data represent the mean ± standard deviation at least three independent experiments. Statistical differences between the groups were assessed using one-way analysis of

variance (ANOVA) or Student's two-tailed paired *t* test in SPSS 13.0 software. A *p*-value of less than .05 (*$p < .05$) was used to indicate statistical differences between the groups.

RESULTS

mDia1 Regulates Activin B-Induced BMSC Migration

To characterize isolated rat BMSCs, we assessed cell surface markers using immunocytochemistry. Supported by previous reports [17, 19], BMSCs were positive for CD29, CD44, and CD90, and nearly negative for CD34 (Supporting Information Fig. S1).

We then investigated whether Activin B regulated mDia1 expression in BMSCs by Western blot analysis. mDia1 expression was remarkably increased at 15 minutes after Activin B stimulation, and decreased after 4 hours (Fig. 1A, 1B).

To analyze the function of mDia1 in Activin B-induced BMSC migration, two mDia1 siRNAs, mDia1-siRNA (1) and mDia1-siRNA (2), which target different nucleotide sequences of mDia1, were individually transfected into BMSCs. Both of the siRNAs reduced the amount of endogenous mDia1 by more than 85% after 24 hours to 48 hours (Fig. 1C, 1D). In a transwell migration assay, as reported previously [11], 10 ng/ml Activin B effectively induced BMSC migration to the lower chamber compared with that of the control group and the NC group. Both mDia1-siRNA (1) and mDia1-siRNA (2) suppressed BMSC migration to the lower chamber with or without Activin B (Fig. 1E, 1F). Consistent with this finding, mDia1-siRNA inhibited BMSC migration induced by Activin B in a scratching wound healing assay (Fig. 1G, 1H). Given that mDia1 siRNAs did not influence BMSC proliferation (Supporting Information Fig. S2), these data showed that mDia1 regulates Activin B-induced BMSC migration.

mDia1 Regulates Activin B-Induced Membrane Ruffles and Microtubule Morphology but Not Activin B-Induced Golgi Reorientation

The coordination of cytoskeletal dynamic changes is important for cell migration, including changes in actin filaments and microtubules [20, 21]. We first assessed the effect of mDia1 on the actin cytoskeleton. We found that Activin B increased the percentage of the leading wound-edge cells with membrane ruffles from ~20%–25% to ~50%. However, mDia1-siRNA inhibited membrane ruffling induced by Activin B (Fig. 2A, 2B). We also found that mDia1 suppression did not inhibit stress fiber formation in BMSCs (Fig. 2A4′).

Rapid reorientation of the Golgi apparatus in the direction of subsequent cell migration could play a role in the production of a new membrane at the leading edge [22]. We found that the percentage of cells with Golgi apparatus facing the edge was 43% ± 5% in the control group, 46% ± 7% in the mDia1-siRNA group, 71% ± 7% in the Activin B group, and 75% ± 6% in the mDia1-siRNA plus Activin B group 8 hours after wounding (Fig. 2C, 2D). These results suggest that Activin B induces reorientation of the Golgi in BMSCs independent of mDia1.

We next analyzed the morphology of microtubules. In contrast to the control cells and the Activin B-treated cells, which adopted an elongated shape with long microtubules toward the wound at the leading edge, there were no comparable number of cells with this structure in the mDia1-suppressed BMSCs with or without Activin B (Fig. 3A, 3B). These data suggest that mDia1 is involved in microtubule morphology in the course of BMSC migration.

mDia1 Coordinates Adhesion Signaling Dynamics

Cell migration involves the continuous formation and disassembly of adhesions (adhesion turnover) [20]. We examined the effect of mDia1-siRNA on focal adhesion signaling dynamics. Western blots revealed that the phosphorylated and total levels of a focal adhesion-associated protein, FAK, peaked in BMSCs at 15 minutes after treatment with Activin B and started to decline at 30 minutes (Fig. 4A, 4B). Total FAK was also increased by Activin B (Fig. 4A, 4C). In addition, another focal adhesion-associated protein, paxillin, was activated at 15 minutes and decreased at 2 hours. However, when mDia1 was inhibited by mDia1-siRNA, FAK, and paxillin were dephosphorylated (Fig. 4A, 4B, 4D). Furthermore, we examined the role of FAK activation in BMSC migration. PF-562271, an inhibitor of FAK, blocked the phosphorylation of FAK and paxillin with or without Activin B (Fig. 4E–4G). We found that PF-562271 suppressed BMSC migration following treatment with Activin B (Fig. 4H, 4I). These data suggest that mDia1 regulates Activin B-induced BMSC migration by integrating adhesion signaling dynamics involving FAK and paxillin.

Cdc42 Is Necessary but Not Sufficient for Activin B-Induced BMSC Migration

Cell migration is critically regulated by Rac1 and Cdc42, two other members of Rho GTPases [23]. We performed a pull-down assay to determine whether Rac1 and Cdc42 were activated by Activin B in BMSCs. We found that GTP-bound Rac1 remained at a constant level with or without Activin B treatment (Fig. 5A, 5B), whereas Cdc42 was activated at 15 minutes after Activin B treatment (Fig. 5A, 5C).

To study the role of Cdc42 in BMSC migration, we transiently transfected the mock vector, the dominant negative mutant of Cdc42 (Cdc42[N17]) or the constitutively active mutant of Cdc42 (Cdc42[L61]) into BMSCs. Cdc42(N17) stopped BMSC migration induced by Activin B. However, Cdc42(L61) did not promote BMSC migration with or without Activin B (Fig. 5D, 5E**)**. These results suggest that Cdc42 is necessary but not sufficient for Activin B-induced BMSC migration.

Cdc42 has been well documented to play key roles in polarity and actin cytoskeleton reorganization [24, 25]. We next detected the role of Cdc42 in Activin B-induced Golgi reorientation and actin reorganization in BMSCs. We found that Cdc42(N17) inhibited Golgi reorientation induced by Activin B at the leading edge from ~74% to ~27% (Fig. 5F). Consistent with this, although the extended elongated invasive shape was readily observed in control cells, this polarized cell shape was hardly seen in the Cdc42(N17)-expressing cells. On the other hand, Cdc42(L61) induced filopodia formation in BMSCs. However, we did not find significant filopodia in BMSCs treated with Activin B (Fig. 5G). Taken together, these data suggest that Cdc42 regulates Activin B-induced BMSC migration and Golgi reorientation at the leading edge.

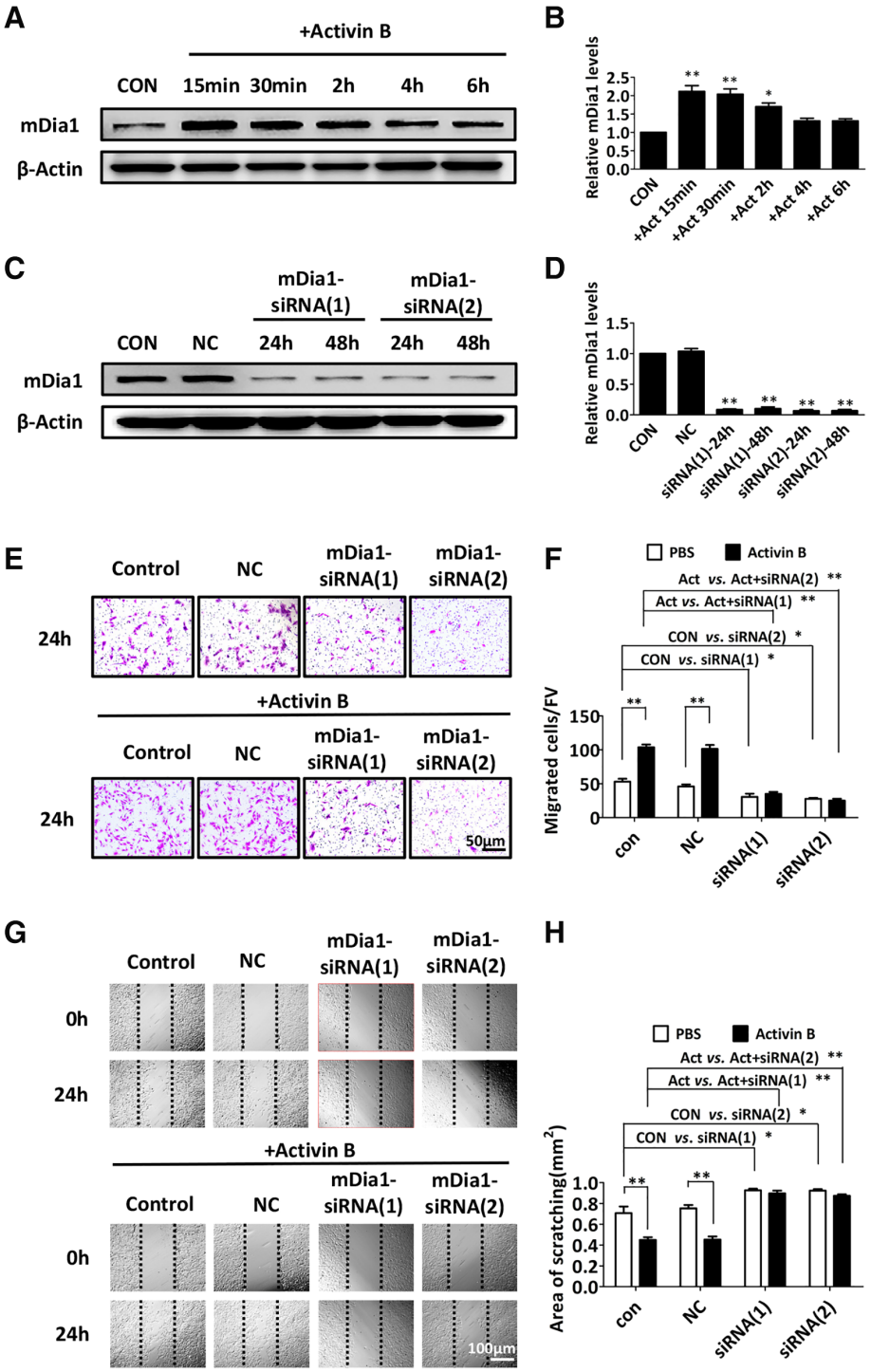

Figure 1. mDia1 regulates bone marrow-derived mesenchymal stromal cell (BMSC) migration induced by Activin B. **(A):** BMSCs were treated without growth factor (control) or with Activin B for the indicated times. Western blotting was performed to analyze mDia1 expression. **(B):** The protein levels of mDia1 were increased prominently by Activin B stimulation. **(C):** BMSCs were transfected with mDia1-siRNA (1), mDia1-siRNA (2), or negative control (NC) and were collected at 0, 24, and 48 hours. Western blot analysis was performed to detect the depletion of mDia1. **(D):** mDia1-siRNA (1) and mDia1-siRNA (2) reduced the amount of endogenous mDia1 by more than 85% after 24–48 hours relative to the control group value. For the transwell migration and wound healing assays, the cells were serum-starved overnight at 24 hours after transfection with NC, mDia1-siRNA (1) or mDia1-siRNA (2). **(E):** Representative images in the transwell assay at 24 hours after migration. **(F):** Statistical analysis of the cell numbers for the transwell assays. **(G):** Representative photographs for the wound healing assays. Cells were cultured in medium with or without Activin B. Photographs were obtained at 0 hours and 24 hours after scratching. **(H):** Quantitative analysis of the area of scratching. The data are representative of three independent experiments. *, $p < .05$ and **, $p < .01$, respectively.

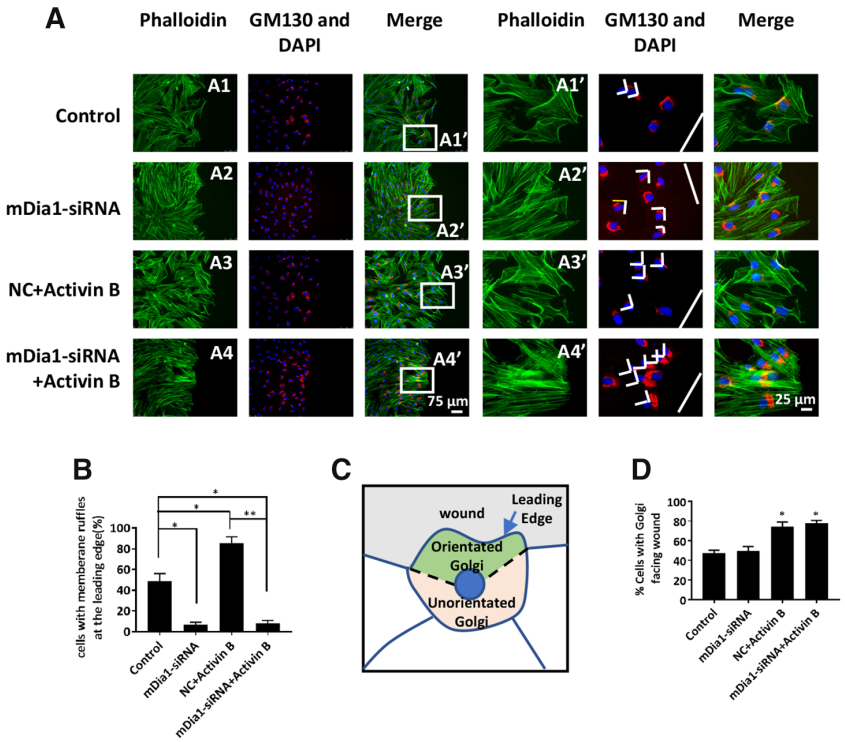

Figure 2. mDia1 regulates Activin B-induced membrane ruffle formation but not the polarization of the Golgi complex at the leading edge of moving bone marrow-derived mesenchymal stromal cells (BMSCs). **(A):** mDia1-siRNA or negative control were used to transfect BMSCs. At 24 hours after transfection, the cells were serum-starved overnight and then cultured in medium without growth factors (control) or with Activin B (10 ng/ml) for the in vitro wound healing assay. After 8 hours of cell migration, BMSCs were fixed, and immunofluorescence was performed with DAPI (blue), phalloidin (green), and anti-GM130 (red). For identification of cells with the Golgi oriented toward the wound, borders and wound edges are depicted in white. **(B):** The percentage of cells showing membrane ruffling at the wound edge was calculated for three independent experiments. For each experiment, more than 100 cells were evaluated. **(C):** A diagram showing the criteria for assessing Golgi reorientation. Lines at a 120° angle representing the front 1/3 and rear 2/3 of the cell area were placed over the nucleus of the cell. Cells were defined as positive if the Golgi was localized within a 120° sector facing directly toward the wound edge. **(D):** Quantitative analysis of cells with Golgi reorientation at the wound edge in three independent experiments. For each experiment, more than 100 cells were evaluated. *, $p < .05$ and **, $p < .01$, respectively, versus control cells.

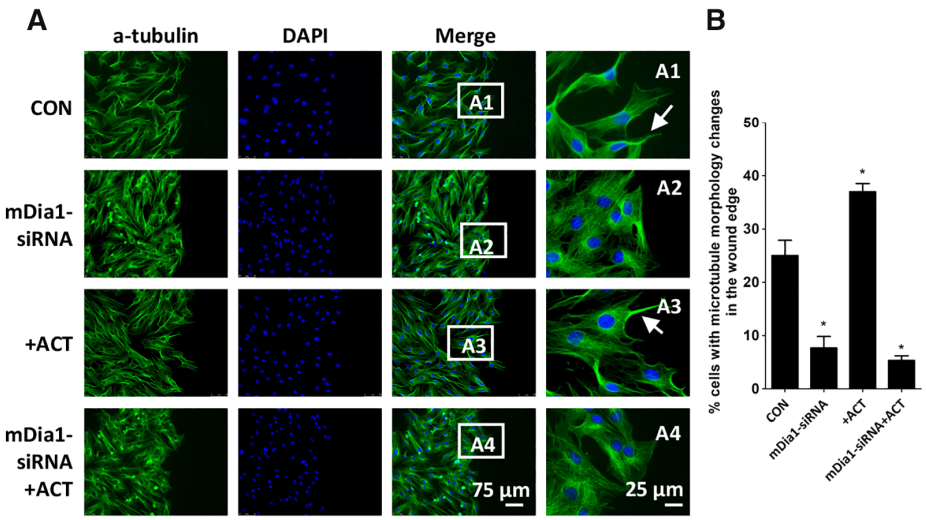

Figure 3. mDia1 regulates the Activin B-induced microtubule morphology of bone marrow-derived mesenchymal stromal cells (BMSCs) at the leading edge. BMSCs were treated as described in Figure 2A. **(A):** After 8 hours of cell migration, cells were fixed, and immunofluorescence was performed with anti-α-tubulin (green) and DAPI (blue). **(B):** The percentage of cells with microtubule morphology changes at the wound edge in three independent experiments. For each experiment, more than 100 cells were evaluated. *, $p < .05$ versus the control group.

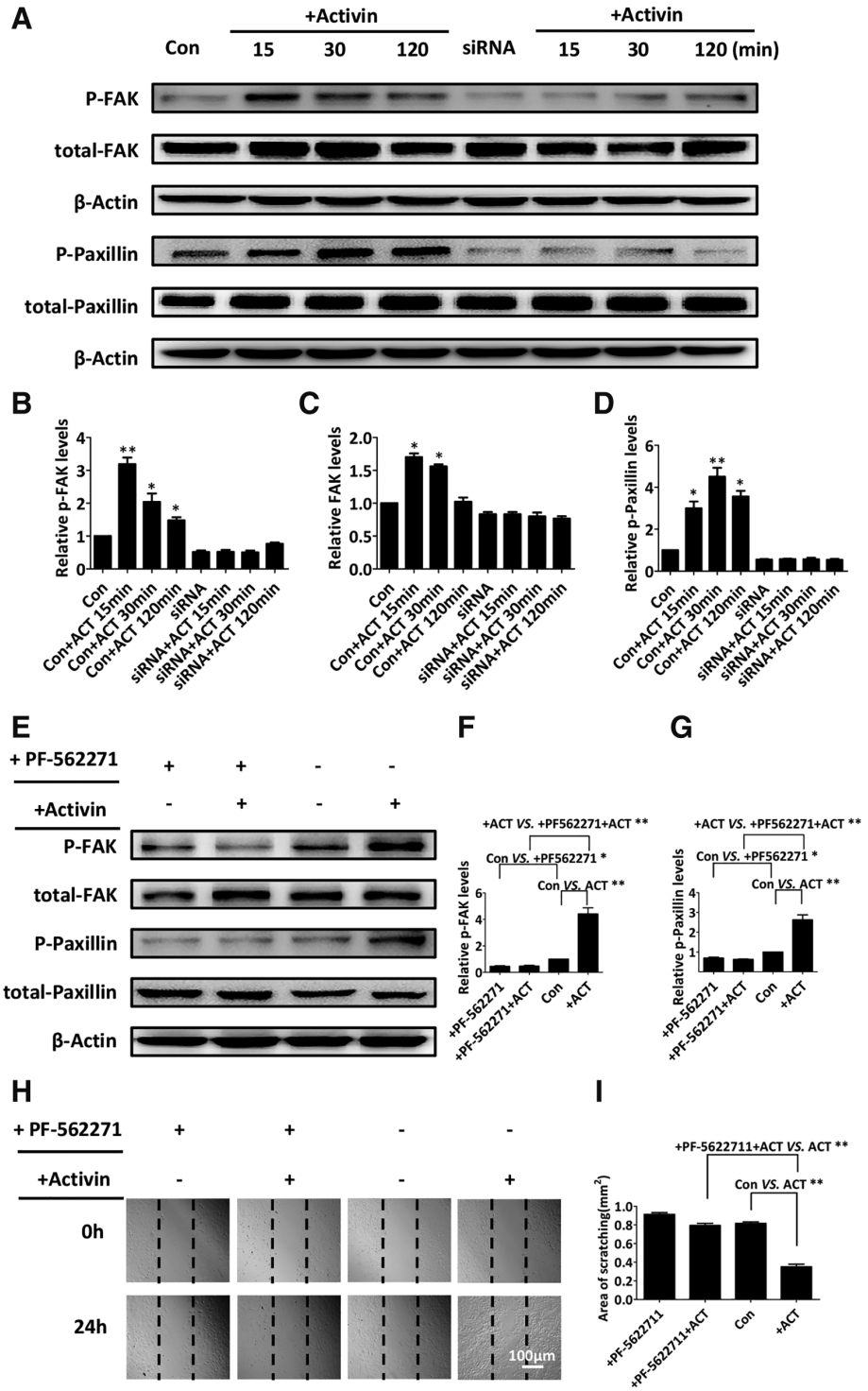

Figure 4. mDia1 coordinates Activin B-induced adhesion signaling dynamics. **(A):** After transfection with or without mDia1-siRNA (1) for 24 hours, bone marrow-derived mesenchymal stromal cells (BMSCs) were serum-starved overnight. The cells were then stimulated without growth factor (control) or with 10 ng/ml of Activin B for the indicated times. Cell lysates were analyzed by Western blotting for phosphorylated and total FAK and paxillin. The ratios of p-FAK versus total FAK **(B)**, total FAK versus β-actin **(C)**, and p-paxillin versus total paxillin **(D)** were calculated and normalized to those of the control group. The data are representative of three independent experiments. **(E):** Cells with or without pretreatment with PF-562271 (5 μM) for 12 hours were incubated in the presence or absence of Activin B for 15 minutes. The levels of phosphorylated and total FAK and paxillin were analyzed by Western blotting. **(F, G):** The ratios of phosphorylated proteins versus total proteins were calculated and normalized to the control group. In the wound scratch assay, BMSCs were treated with or without Activin B in the presence or absence of the inhibitor PF-562271 (5 μM). **(H):** Photographs were obtained immediately and 24 hours after wounding. **(I):** The area of scratching was calculated. The data are representative of three independent experiments. *, $p < .05$ and **, $p < .01$, respectively

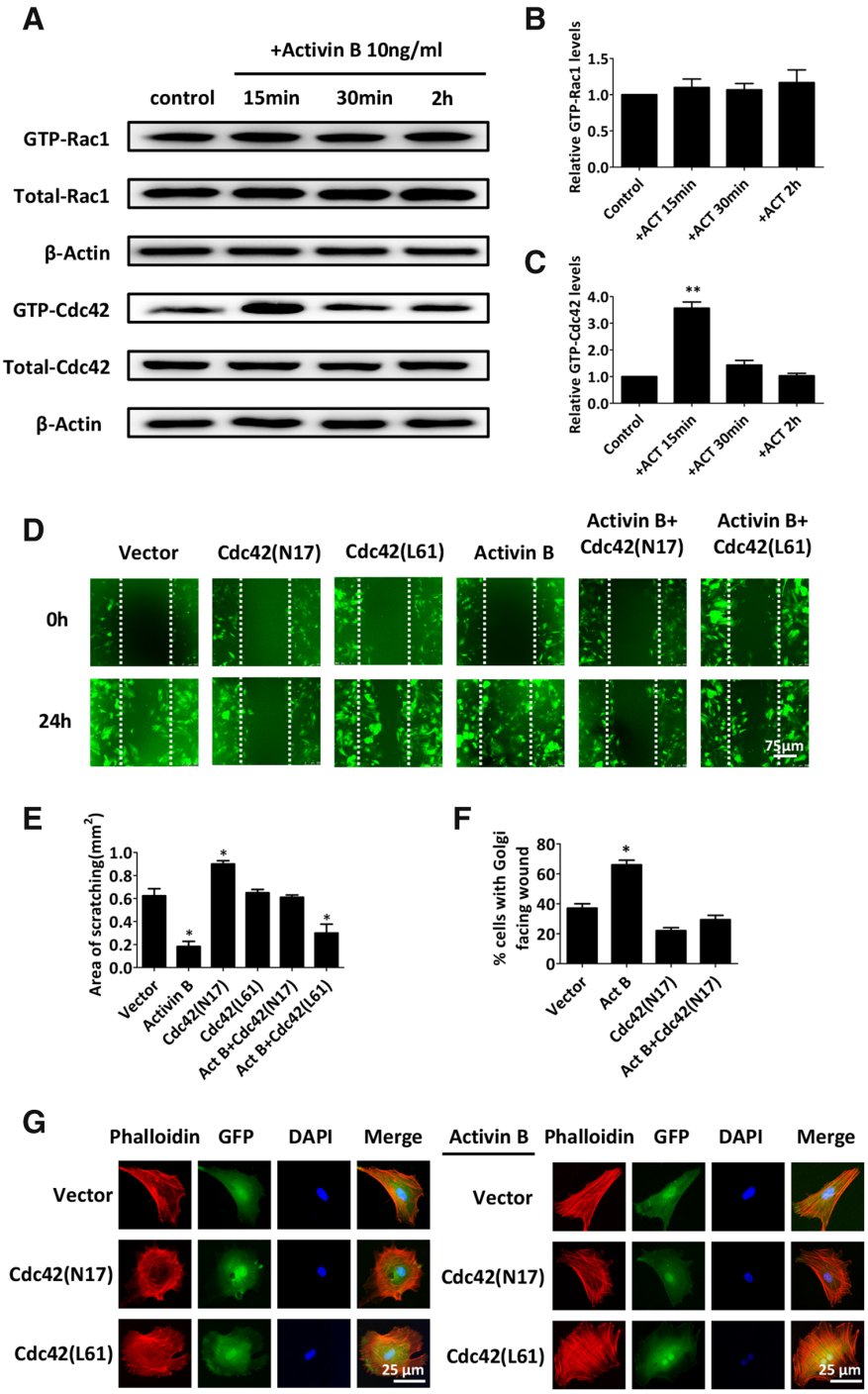

Figure 5. Cdc42 is necessary but not sufficient for bone marrow-derived mesenchymal stromal cell (BMSC) migration induced by Activin B. **(A):** Pull-down assays were performed to detect the amounts of GTP-bound Rac1 and Cdc42 in BMSCs treated with phosphate buffered solution or Activin B for the indicated times. The ratios of GTP-Rac1 versus total Rac1 **(B)** and GTP-Cdc42 versus total Cdc42 **(C)** were quantified and normalized to those of the control group. In the wound healing assays, BMSCs were transduced with vector lentivirus, Cdc42(N17) or Cdc42(L61) for 48 hours and starved overnight. Wound healing assays were performed in the cells in the presence or absence of Activin B. representative images **(D)** and quantification **(E)** of the wound healing assays at 0 hours and 24 hours after scratching. To analyze the role of Cdc42 in Golgi reorientation in BMSC migration, immunofluorescence staining was performed with anti-GM130 and DAPI after 8 hours of cell migration (data not shown); the percentage of cells with Golgi reorientation at the wound edge is shown in **(F)**. **(G):** In rhodamine-phalloidin staining, BMSCs were treated as in Fig. 4D. Then, the cells were cultured in medium with or without Activin B for 4 hours. the cells were fixed and immunofluorescence was performed with rhodamine-phalloidin (red) and DAPI (blue). GFP fluorescence indicates the virus-infected cells. *, $p < .05$ versus the vector group. **, $p < .01$ versus the control group

mDia1 Promotes Activin B-Induced BMSC-Mediated Skin Wound Healing In Vivo

A full-thickness wound healing model was established in rats to explore whether knockdown of mDia1 affected BMSC-mediated wound healing in vivo. After wounding, rats were randomly divided into six groups. The wounds of each group were treated with PBS (control), Activin B, BMSCs, Activin B + BMSCs, BMSCs transfected with lentivirus containing shRNA targeting mDia1 (BMSC[mDia1-shRNA]), or Activin B + BMSC(mDia1-shRNA). The efficient transduction of mDia1-shRNA was confirmed by GFP imaging and Western blot analysis (Supporting Information Fig. S3). To assess BMSCs administered to the rat tissue, we collected the frozen sections on day 3 after BMSC transplantation. Green fluorescence ($EGFP^+$) cells were detected in the frozen sections of the BMSC group, ACT + BMSC group, BMSC(mDia1-shRNA) group, and ACT + BMSC(mDia1-shRNA) group but not in the Activin B group or PBS (control) group (Supporting Information Fig. S4). These data suggest that BMSCs were incorporated into wound sites on day 3 after transplantation. In addition, some green fluorescence ($EGFP^+$)-expressing cells began to migrate to other locations of the wound from the site of the transplanted cell mass in the BMSC group and the Activin B + BMSC group (white arrow in Supporting Information Fig. S4). However, we did not find comparable migrated cells in the BMSC(mDia1-shRNA) group or the ACT + BMSC (mDia1-shRNA) group.

Wound closure rates were then evaluated. As we reported before [6], compared with that of the control group, Activin B group and BMSC group, the rates of skin wound closure in the Activin B + BMSC group were significantly accelerated. However, the wound closure rates in the BMSC(mDia1-shRNA) group were lower than those in the BMSC group on days 3 and 7 after treatment. The wound healing rate in the Activin B + BMSC(mDia1-shRNA) group was also decreased compared with that of the Activin B + BMSC group (Fig. 6A, 6B). These data suggest that mDia1 inhibition in BMSCs inhibited in vivo wound healing induced by Activin B + BMSCs.

We then evaluated re-epithelialization and granulation tissue formation, two critical milestones of the wound healing process, according to the criteria described in Supporting Information Table S1. A semiquantitative histological score of 1–3 ($\pm$0.5) was given for re-epithelialization and granulation tissue formation for each wound. The epidermal layers showed keratinization in all six groups 14 days postwounding. There was no significant difference in the re-epithelialization scores of six groups at this stage (Fig. 6C, 6D). Mature granulation is characteristic of a more advanced healing stage. Transformation of immature granulation tissue into mature granulation tissue is characterized by elongation of fibroblasts, deposition of collagen fibers, formation of new matrix fibers, and angiogenesis [26]. The granulation tissue scores of the BMSC and Activin B + BMSC groups were much higher than those of the other four groups (Fig. 6C, 6E). We found that the matrix fiber pattern in the Activin B plus BMSC group was similar to that in normal skin at the wound gap. However, the granulation tissue in the BMSC(mDia1-shRNA) group was significantly less mature than that in the BMSC group. Similarly, mature granulation tissue formation in the Activin B + BMSC(mDia1-shRNA) group was delayed compared with that in the Activin B + BMSC group. Collectively, these data suggest that mDia1 promotes Activin B-induced BMSC-mediated wound healing and granulation tissue maturation in vivo.

Discussion

In our previous study, we found that RhoA activation plays a crucial role in Activin B-induced migration of BMSCs independent of the RhoA effector ROCK [11]. Here, we showed that mDia1, another RhoA effector, regulates Activin B-induced migration of BMSCs. Given that inhibition of ROCK promotes but inhibition of mDia1 suppresses BMSC migration, ROCK, and mDia1 appear to play opposite roles in Activin B-induced migration of BMSCs. Consistent with our findings, opposing actions of mDia1 and ROCK have been reported in other cells. For example, mDia1 promotes RhoA-induced migration of human dental pulp cells, but ROCK has the opposite effect [27]. Tsuji et al. also found that ROCK and mDia1 have antagonizing functions in membrane ruffle formation in Swiss3T3 fibroblasts [28]. In epithelial cells, Sahai et al. found that ROCK disrupts but mDia1 maintains adherent junctions downstream of Rho [29].

The coordinated regulation of actin, microtubules, and adhesion sites is essential in the efficient migration process [8, 20, 21]. The present study suggests that the RhoA-mDia1 signaling circuit plays a key role in Activin B-induced membrane ruffling, microtubule morphology, and adhesion signaling dynamics in BMSCs. Our data are consistent with previous findings that mDia controls actin polymerization and mediates Rho-regulated formation and orientation of stable microtubules [30, 31]. Our data also support the findings of Zaoui et al. that Memo-RhoA-mDia1 signaling regulates the coordination of the organization of the lamellipodial actin network, adhesion formation, and microtubule outgrowth at the leading edge in the cell migration of SKBR3 and T47D breast carcinoma cells [32]. In addition, our data are suggestive of the importance of the FAK pathway in PGE2-induced migration of mesenchymal stem cells [33]. However, in contrast to our finding that mDia1 suppression does not inhibit stress fiber formation in BMSCs, Satoh and Tominaga found that mDia induces stress fiber formation in HeLa cells [34]. These data suggest that the effect of mDia1 in stress fiber formation is cell type-dependent.

In addition to RhoA, Rac1, and Cdc42 also play important roles in cell migration [8]. Our study showed that Rac1 activity did not change upon Activin B treatment of BMSCs. However, given the importance of the spatiotemporal dynamics of Rac1 activity in cell migration [35], we cannot rule out the possibility that Rac1 is involved in Activin B-induced BMSC migration, which may be revealed by detection of the distribution of GTP-Rac1 in Activin B-treated BMSCs.

In response to certain external cues, cells reorganize their cytoskeleton to achieve polarization, including Golgi reorientation, which promotes directional migration toward the cues [36]. In this study, we found that Activin B promotes Golgi reorientation at the leading edge of moving BMSCs 8 hours after wounding. However, the Golgi reorientation induced by Activin B is not mediated by mDia1. This result is in contrast to the previous finding that mDia1 depletion impairs directed migration by inhibiting cell polarization in rat C6 glioma [37], suggesting that whether mDia1

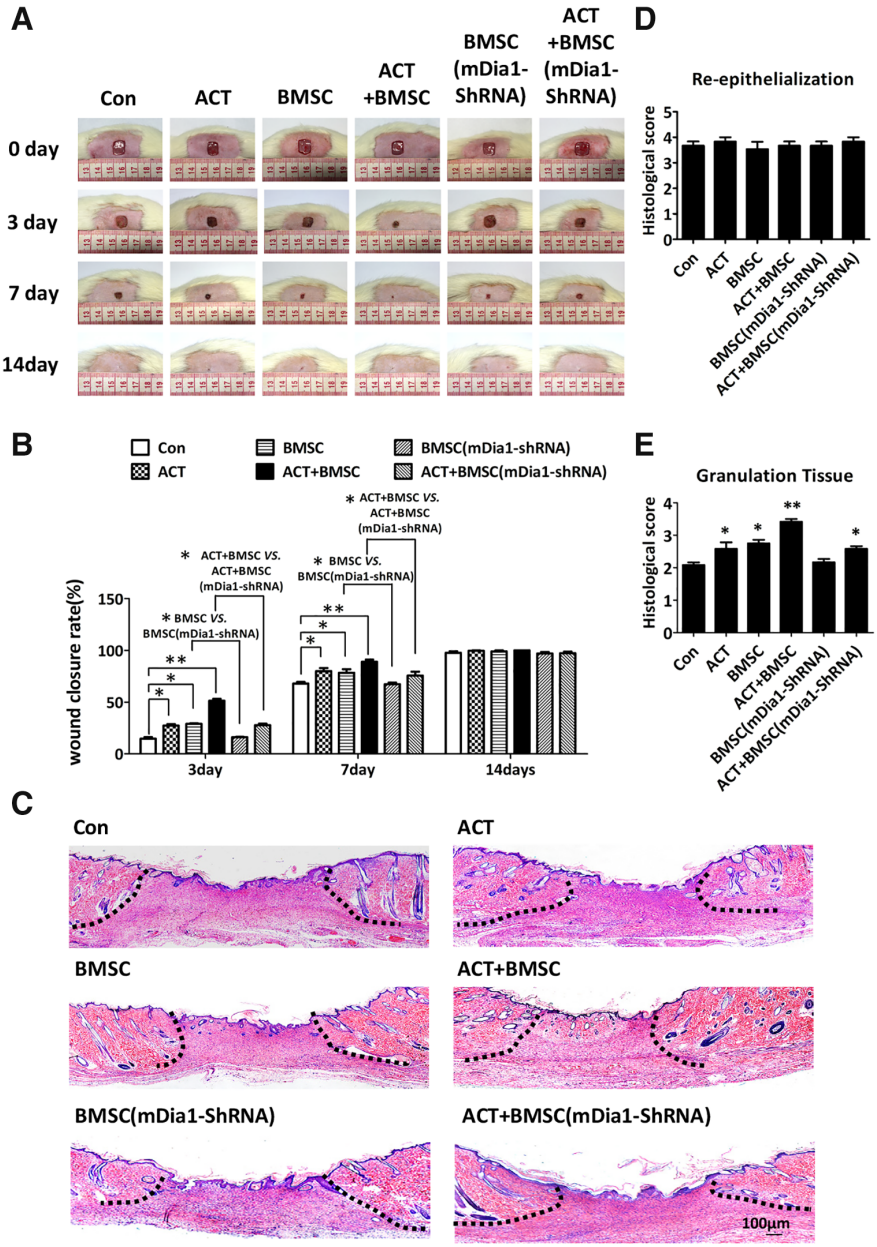

Figure 6. mDia1 regulates Activin B-induced bone marrow-derived mesenchymal stromal cell-mediated skin wound healing in vivo. Six groups of rats were administered as described in the methods section. **(A):** Representative photographs of wounds in six groups taken at 0, 3, 7, and 14 days after wounding. **(B):** Quantification of the wound closure rate among the six groups (n = 6). **(C):** HE staining shows the re-epithelialization and granulation tissue formation of the six groups on day 14 after wounding. Black dotted lines indicate a border between the normal dermis and wound gap. Histological scores of re-epithelialization **(D)** and granulation tissue formation **(E)** were evaluated by the criteria in Supporting Information Table S1. *, $p < .05$ and **, $p < .01$, respectively, versus control group.

regulates cell polarization is cell type-dependent, similar to its role in stress fiber formation. However, our data suggest that Activin B-induced Golgi reorientation in BMSCs is regulated by Cdc42. Consistent with these findings, BMSCs transfected with Cdc42(N17) lost the polarized cell shape. These results support the well-established role of Cdc42 in mediating polarization of the Golgi complex in front of the nucleus in a moving cell [24]. Our data are also consistent with the findings by Friesland et al. that Cdc42 inhibition disrupts GM130-docked Golgi structures and suppresses cell motility [38].

The ability of mesenchymal stem cells to enhance cutaneous wound healing has been well characterized [3]. In this study, we found that mDia1 plays a role in BMSC-induced wound healing in vivo, as evidenced by the reduced wound healing rate and impaired granulation tissue formation upon mDia1 suppression. Given that Ptx3-deficient MSCs delay wound closure and reduce granulation tissue formation [39], it appears that both mDia1 and Ptx3 are important for wound healing.

In this study, we demonstrated that BMSCs applied to the rat tissue could migrate to other locations of the wound bed

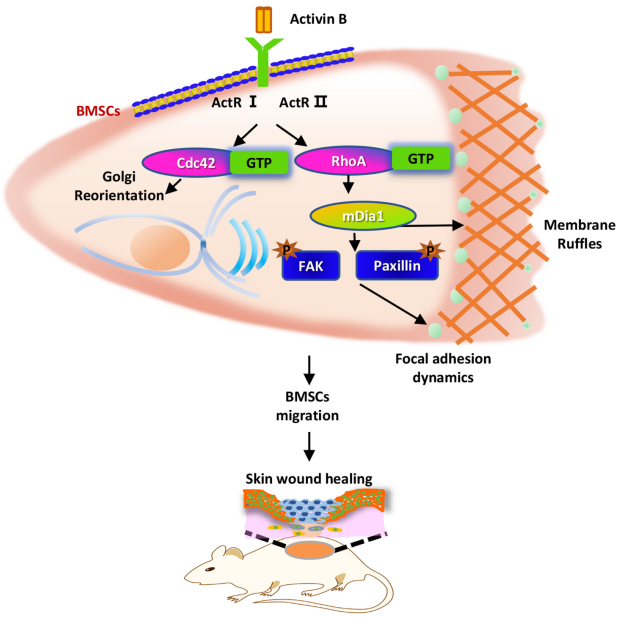

Figure 7. Model of the mechanisms of RhoA-mDia1- and Cdc42-regulated Activin B-induced bone marrow-derived mesenchymal stromal cell (BMSC) migration. The RhoA-mDia1 pathway regulates Activin B-induced BMSC migration by promoting membrane ruffling, microtubule morphology and focal adhesion signaling dynamics. Cdc42 mediates Activin B-induced Golgi complex polarization at the leading edge of moving BMSCs. mDia1 is involved in the wound healing process mediated by BMSCs and induced by Activin B.

3 days after transplantation. This phenomenon suggests that the migration of injected BMSCs to the damaged tissues may be a key event in the participation of these cells in tissue repair. Thus, BMSCs with a high migratory ability may be able to migrate to the entire wound bed faster and perform biological functions in a larger area compared with BMSCs with low migration ability. This may explain why BMSCs with a high migratory ability could effectively promote wound healing in our study. Therefore, understanding the mechanism of BMSC migration will help us optimize clinical MSC-based transplantation strategies to promote skin wound healing.

In our previous and present studies, we demonstrated that RhoA, mDia1, and even Cdc42, could regulate the formation of the cytoskeleton, even cell shape, in rat BMSCs. Taken that the changes in cell shape and the integrity of the cytoskeleton appear to be important in stem cell differentiation [40], we propose that Activin B-induced RhoA and mDia1 activation may affect BMSC differentiation capacity in the skin wound healing process, in addition to their regulation of BMSC migration. In support of this hypothesis, McBeath et al. found that RhoA mediated the shape-dependent control of human MSC commitment to the osteoblast or adipocyte lineages [41]. A recent study also found that TGFβ-activated RhoA signaling plays a key role in regulating the fate of MSCs in arterial repair after injury [42].

Furthermore, compared with normally healing wounds, chronic and nonhealing wounds are a more challenging problem. BMSC-based therapy has shown efficacy in nonhealing wounds [43]. In this study, we found that Activin B plus BMSCs promoted wound healing. We propose that the combination of Activin B and BMSCs may also have potential for treatment of chronic nonhealing skin wounds. However, considering the complex environment in the chronic wound and the characteristics of growth factors, which are easy to degrade, a controlled release delivery system should be constructed for use of Activin B in chronic and nonhealing wounds.

Conclusion

In this study, we revealed that the RhoA-mDia1 pathway regulates Activin B-induced BMSC migration by promoting membrane ruffling, microtubule morphology, and focal adhesion signaling dynamics. Cdc42 mediates Activin B-induced polarization of the Golgi complex at the leading edge of moving BMSCs. In addition, mDia1 in BMSCs is essential for granulation tissue maturation and skin wound healing induced by Activin B. Our findings may be of clinical significance for tissue regenerative therapies.

Acknowledgments

This work was supported by the National Natural Science Foundation of China (81872514, 81571860, 81430045, and 81703147) and the Colleges Pearl River Scholar Funded Scheme (GDUPS2013 and GDUPS2015). The project is also supported by the Natural Science Foundation of Guangdong Province (2014A030312013 and 2017A030-310292).

Author Contributions

X.W.: conception and design, collection and assembly of data, data analysis and interpretation, and article writing; P.T.: collection of data; F.G.: article writing; M.Z. and M.H.: data analysis and interpretation; Y.Y. and Y.C.: provision of administrative support; L.Z.: conception and design, financial support, and final approval of the article; L.Z.: conception and design, financial support, article writing, and final approval of the article.

Disclosure of Potential Conflicts of Interest

The authors indicated no potential conflicts of interest.

References

1 Jiang Y, Jahagirdar BN, Reinhardt RL et al. Pluripotency of mesenchymal stem cells derived from adult marrow. Nature 2002;418:41–49.

2 Maxson S, Lopez EA, Yoo D et al. Concise review: role of mesenchymal stem cells in wound repair. Stem Cells Translational Medicine 2012;1:142–149.

3 Motegi SI, Ishikawa O. Mesenchymal stem cells: the roles and functions in cutaneous wound healing and tumor growth. J Dermatol Sci 2017;86:83–89.

4 Chen JS, Wong VW, Gurtner GC. Therapeutic potential of bone marrow-derived mesenchymal stem cells for cutaneous wound healing. Front Immunol 2012;3:192.

5 Pauklin S, Vallier L. Activin/nodal signalling in stem cells. Development 2015;142: 607–619.
6 Zhang M, Sun L, Wang X et al. Activin B promotes BMSC-mediated cutaneous wound healing by regulating cell migration via the JNK-ERK signaling pathway. Cell Transplant 2014;23:1061–1073.
7 Machacek M, Hodgson L, Welch C et al. Coordination of Rho GTPase activities during cell protrusion. Nature 2009;461: 99–103.
8 Ridley AJ. Rho GTPase signalling in cell migration. Curr Opin Cell Biol 2015;36: 103–112.
9 Hall A. Rho family GTPases. Biochem Soc Trans 2012;40:1378–1382.
10 Narumiya S, Tanji M, Ishizaki T. Rho signaling, ROCK and mDia1, in transformation, metastasis and invasion. Cancer Metastasis Rev 2009;28:65–76.
11 Wang X, Tang P, Guo F et al. RhoA regulates Activin B-induced stress fiber formation and migration of bone marrow-derived mesenchymal stromal cell through distinct signaling. Biochim Biophys Acta 2017;1861: 3011–3018.
12 Lotfy A, Salama M, Zahran F et al. Characterization of mesenchymal stem cells derived from rat bone marrow and adipose tissue: a comparative study. Int J Stem Cells 2014;7:135–142.
13 Tian Z, Lv X, Zhang M et al. Deletion of epithelial cell-specific Cdc42 leads to enamel hypermaturation in a conditional knockout mouse model. Biochim Biophys Acta 2018; 1864:2623–2632.
14 Zhang L, Wang W, Hayashi Y et al. A role for MEK kinase 1 in TGF-beta/activin-induced epithelium movement and embryonic eyelid closure. EMBO J 2003;22:4443–4454.
15 Woodham EF, Paul NR, Tyrrell B et al. Coordination by Cdc42 of Actin, contractility, and adhesion for melanoblast movement in mouse skin. Curr Biol 2017;27: 624–637.
16 Galiano RD, Michaels J, Dobryansky M et al. Quantitative and reproducible murine model of excisional wound healing. Wound Repair Regen 2004;12:485–492.
17 Wu Y, Chen L, Scott PG et al. Mesenchymal stem cells enhance wound healing through differentiation and angiogenesis. Stem Cells 2007;25:2648–2659.
18 Braiman-Wiksman L, Solomonik I, Spira R et al. Novel insights into wound healing sequence of events. Toxicol Pathol 2007;35: 767–779.
19 McFarlin K, Gao X, Liu YB et al. Bone marrow-derived mesenchymal stromal cells accelerate wound healing in the rat. Wound Repair Regen 2006;14:471–478.
20 Ridley AJ, Schwartz MA, Burridge K et al. Cell migration: integrating signals from front to back. Science 2003;302:1704–1709.
21 Etienne-Manneville S. Microtubules in cell migration. Annu Rev Cell Dev Biol 2013; 29:471–499.
22 Yadav S, Linstedt AD. Golgi positioning. Cold Spring Harb Perspect Biol 2011;3: 725–738.
23 Sadok A, Marshall CJ. Rho GTPases: masters of cell migration. Small GTPases 2014;5: e29710.
24 Etienne-Manneville S. Cdc42—the centre of polarity. J Cell Sci 2004;117:1291–1300.
25 Murali A, Rajalingam K. Small Rho GTPases in the control of cell shape and mobility. Cell Mol Life Sci 2014;71:1703–1721.
26 Tkalcevic VI, Cuzic S, Parnham MJ et al. Differential evaluation of excisional non-occluded wound healing in db/db mice. Toxicol Pathol 2009;37:183–192.
27 Cheng L, Xu J, Qian YY et al. Interaction between mDia1 and ROCK in Rho-induced migration and adhesion of human dental pulp cells. Int Endod J 2017;50:15–23.
28 Tsuji T, Ishizaki T, Okamoto M et al. ROCK and mDia1 antagonize in Rho-dependent Rac activation in Swiss 3T3 fibroblasts. J Cell Biol 2002;157:819–830.
29 Sahai E, Marshall CJ. ROCK and Dia have opposing effects on adherens junctions downstream of Rho. Nat Cell Biol 2002;4: 408–415.
30 Kovar DR, Harris ES, Mahaffy R et al. Control of the assembly of ATP- and ADP-actin by formins and profilin. Cell 2006; 124:423–435.
31 Palazzo AF, Cook TA, Alberts AS et al. mDia mediates Rho-regulated formation and orientation of stable microtubules. Nat Cell Biol 2001;3:723–729.
32 Zaoui K, Honore S, Isnardon D et al. Memo-RhoA-mDia1 signaling controls microtubules, the actin network, and adhesion site formation in migrating cells. J Cell Biol 2008;183:401–408.
33 Lu X, Han J, Xu X et al. PGE2 promotes the migration of mesenchymal stem cells through the activation of FAK and ERK1/2 pathway. Stem Cells Int 2017;2017: 8178643.
34 Satoh S, Tominaga T. mDia-interacting protein acts downstream of Rho-mDia and modifies Src activation and stress fiber formation. J Biol Chem 2001;276: 39290–39294.
35 Kurokawa K, Nakamura T, Aoki K et al. Mechanism and role of localized activation of Rho-family GTPases in growth factor-stimulated fibroblasts and neuronal cells. Biochem Soc Trans 2005;33:631–634.
36 Kupfer A, Louvard D, Singer SJ. Polarization of the Golgi apparatus and the microtubule-organizing center in cultured fibroblasts at the edge of an experimental wound. Proc Natl Acad Sci U S A 1982;79: 2603–2607.
37 Yamana N, Arakawa Y, Nishino T et al. The Rho-mDia1 pathway regulates cell polarity and focal adhesion turnover in migrating cells through mobilizing Apc and c-Src. Mol Cell Biol 2006;26: 6844–6858.
38 Friesland A, Zhao Y, Chen YH et al. Small molecule targeting Cdc42-intersectin interaction disrupts Golgi organization and suppresses cell motility. Proc Natl Acad Sci U S A 2013;110:1261–1266.
39 Cappuzzello C, Doni A, Dander E et al. Mesenchymal stromal cell-derived PTX3 promotes wound healing via fibrin remodeling. J Invest Dermatol 2016;136:293–300.
40 Treiser MD, Yang EH, Gordonov S et al. Cytoskeleton-based forecasting of stem cell lineage fates. Proc Natl Acad Sci U S A 2010;107:610–615.
41 McBeath R, Pirone DM, Nelson CM et al. Cell shape, cytoskeletal tension, and RhoA regulate stem cell lineage commitment. Dev Cell 2004;6:483–495.
42 Li C, Zhen G, Chai Y et al. RhoA determines lineage fate of mesenchymal stem cells by modulating CTGF-VEGF complex in extracellular matrix. Nat Commun 2016;7:11455.
43 Chen S, Shi J, Zhang M et al. Mesenchymal stem cell-laden anti-inflammatory hydrogel enhances diabetic wound healing. Sci Rep 2015;5:18104.

See www.StemCells.com for supporting information available online.